Particle simulation of three-dimensional convection patterns in a Rayleigh-Bénard system

Tadashi Watanabe and Hideo Kaburaki
Research and Development Group for Numerical Experiments, Japan Atomic Energy Research Institute, Tokai-mura, Naka-gun, Ibaraki-ken, 319-11, Japan
(Received 11 April 1997)

The transition of convection patterns in the three-dimensional Rayleigh-Bénard system is simulated using the direct simulation Monte Carlo method. The simulation region is a rectangular box with an aspect ratio of 8:8:1, and the number of simulation particles is 2.048×10^7. A hexagonal flow pattern is observed in the convection state with the Rayleigh number slightly higher than the critical value. It is found that the hexagonal flow pattern evolves into a roll pattern with an increase in the Rayleigh number. A hysteresis is seen in the transition between the hexagonal and roll patterns. [S1063-651X(97)12407-2]

PACS number(s): 02.70.−c, 47.54.+r, 05.70.Ln, 47.20.Bp

I. INTRODUCTION

The Rayleigh-Bénard (RB) system, in which a fluid is contained between two horizontal parallel walls and the bottom wall is kept at a higher temperature than the top wall, is one of the most representative nonequilibrium hydrodynamic systems. In the RB system, a heat conduction state is established when the temperature difference between the top and bottom walls is smaller than a critical value, while convection rolls appear when the temperature difference exceeds the critical value. Convection in the RB system has been extensively studied both experimentally and numerically, and reviewed by Ahlers [1], and Cross and Hohenberg [2]. Recent efforts to describe complex spatiotemporal convection patterns in the RB system were briefly reviewed by Pesch [3]. The RB convection has been studied using particle simulation methods such as the molecular dynamics (MD) method and the direct simulation Monte Carlo (DSMC) method in order to study the microscopic behavior of the macroscopic flow. The RB convection was simulated using the MD method by Mareschal and Kestemont [4,5], and Rapaport [6]. Mareschal *et al.* [7], Puhl, Mansour, and Mareschal [8], and Given and Clementi [9] compared the field variables in the convection rolls obtained by the MD method with the results by the hydrodynamic calculations. The chaotic motion of atoms in the transition between heat conduction and convection was studied using the MD method by Watanabe and Kaburaki [10]. Posch, Hoover, and Kum studied the RB problem using the smooth-particle applied mechanics (SPAM), which is a grid-free particle method for solving the partial differential equations of fluid or solid mechanics [11,12]. The good agreement between the smooth-particle and the Navier-Stokes results was obtained, and SPAM was shown to be an interesting bridge between continuum mechanics and molecular dynamics [13]. The convection rolls were also simulated using the DSMC method by Garcia [14], and Stefanov and Cercignani [15]. Garcia and Penland [16] compared velocity distributions in the convection rolls with the numerical solution of the Navier-Stokes equations. The transition between conduction and convection was shown by Watanabe, Kaburaki, and Yokokawa using the DSMC method [17], and the spatial correlations of temperature fluctuations were shown to grow in the transition [18]. Through these studies, the macroscopic flow phenomena in the RB system were shown to be simulated qualitatively and quantitatively using the particle simulation methods. These microscopic simulations were, however, performed in a two-dimensional region with a small aspect ratio, since a large number of particles are necessary to simulate a three-dimensional flow or even the two-dimensional flow with a large aspect ratio. In this paper, the DSMC method is applied to simulate the RB system in a three-dimensional rectangular box with an aspect ratio of 8:8:1. The transition between conduction and convection and the formation of convection patterns are discussed, and the applicability of the DSMC method to macroscopic flow transitions or instabilities is studied.

II. SIMULATION CONDITIONS

In the DSMC method [19], a large number of molecules in a real gas are simulated by a smaller number of representative particles. The trajectories of the particles are traced in a short-time interval by decoupling interparticle collisions, and the collisions take place on a probabilistic basis. Macroscopic quantities are obtained by sampling particle properties in a small volume called sampling cell.

The simulation region is a three-dimensional rectangular box, which is 44.8 mm in horizontal directions and 5.6 mm in vertical direction, filled with hard sphere particles with a diameter of 3.7×10^{-10} m and a mass of 4.8×10^{-26} kg. These particles simulate the average molecule of air. The Prandtl number is estimated to be 0.67 from the Chapman-Enskog theory for spherically symmetrical molecules [20]. The initial temperature and pressure are assumed to be 80 K and 20 Pa, respectively. Under these conditions, the number density is 1.81×10^{22} m^{-3}, the mean free path is 0.091 mm, and the Knudsen number is estimated to be 0.016. The simulation region is divided into $160\times160\times20$ sampling cells. In our simulation, the collision process of the DSMC method is calculated in the sampling cell. Initially, each sampling cell contains 40 particles, and the number of all simulation particles is 2.048×10^7. The DSMC program is parallelized and executed on Intel Paragon with 128 processors. The time step is chosen to be 0.5 of the mean free time. A sampling is performed in every two simulation time steps, and a flow

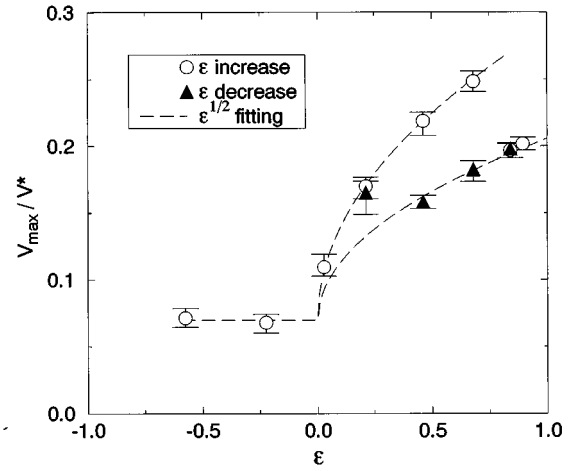

FIG. 1. Maximum vertical velocity in the steady state as a function of $\varepsilon=(R-R_c)/R_c$, where R is the Rayleigh number and R_c is its critical value. The data points show a long-time average in the steady state and the error bars indicate the range of data distribution. The dashed lines indicate fitting curves of $\varepsilon^{1/2}$ for increasing and decreasing ε.

field is obtained by an average of 200 samplings.

The temperature of the bottom wall is slightly increased at time zero from the initial value, and the simulation is performed for thousands of time steps with this temperature condition. The bottom wall temperature is then slightly increased and the simulation is performed again. After the bottom wall temperature reaches a specified value, the simulation is performed for tens of thousands of time steps until the steady state flow field is established. The temperature of the top wall is unchanged. In our simulation, the specified values for the temperature of the bottom wall are 200 K, 300 K, 400 K, 500 K, 700 K, 1000 K, 1400 K, and 1600 K. After the steady state is obtained for the maximum specified temperature, the temperature of the bottom wall is decreased to the smaller specified value, and the simulation is performed until the steady state is established. In this way, simulations with a different temperature condition are performed. The diffuse reflection boundary condition, in which a reflected particle has the velocity components randomly sampled from the Maxwellian distribution corresponding to the surface temperature, is assumed at the top and bottom walls, while the cyclic boundary condition is applied at the side boundaries. The gravitational acceleration is chosen to be a hypothetical value so as to minimize density variations in the heat conduction state [11]: $g=(k_B\Delta T)/(mL_z)$, where k_B is the Boltzmann constant, ΔT the temperature difference, m the particle mass, and L_z the distance between the top and bottom walls.

III. CONVECTION FLOW FIELD

The maximum flow velocity in the vertical direction is shown in Fig. 1 as a function of ε, where ε is defined by $\varepsilon=(R-R_c)/R_c$, R is the Rayleigh number, and R_c is the critical Rayleigh number. The Rayleigh number for this system is given by $R=256/(125\pi)(\Delta T/T)^2(L_z/\lambda)^2$ based on the Chapman-Enskog theory [20], where T is the average temperature and λ is the mean free path. The critical Rayleigh number is defined above which convection states appear and is determined from the simulation results. The maximum velocity is normalized by the reference velocity, which is defined as the average thermal speed for the average temperature in the system, $v^*=(8k_BT)^{1/2}/(m\pi)^{1/2}$. The data points show a long-time average in the steady state. The error bars indicate the range of data distribution due to the statistical simulation conditions such as the number of simulation particles and samplings. The standard deviation is, however, much smaller than the size of each data point.

In the heat conduction state for $\varepsilon<0$, no large-scale flow is established in the system. The maximum flow velocity is, however, not zero in the heat conduction state as shown in Fig. 1. The DSMC data in this region show almost the same velocity, which does not depend on ε. These nonzero velocities are thus due to the statistical simulation conditions. The maximum flow velocity increases as ε increases in the convection state for $\varepsilon>0$. A hexagonal convection pattern is observed when ε is relatively small. It is found, however, that the maximum velocity is suddenly decreased at around $\varepsilon=0.75$ due to the transition of convection states from hexagonal to roll pattern. After the transition, the maximum flow velocity increases again with ε as shown in Fig. 1. If ε is decreased in the convection state with the roll pattern, the roll pattern is observed even at the smaller ε than 0.75. In this condition the maximum flow velocity is smaller than that observed for increasing ε. The transition of convection states from roll to hexagonal pattern is found at around $\varepsilon=0.3$. The hysteresis in the transition of convection states between hexagonal and roll patterns is also observed in the experiments [21,22].

In a region near the onset of convection, a convecting flow velocity is shown to grow as $\varepsilon^{1/2}$ from the perturbation theory for the hydrodynamic equations [23]. Two fitting curves of $\varepsilon^{1/2}$ to the DSMC results are shown in Fig. 1: one is for increasing ε and the other is for decreasing ε. The good agreement between the microscopic DSMC results and the macroscopic hydrodynamic theory is shown in Fig. 1. The critical Rayleigh number of this system, which is obtained from the fitting curves at $\varepsilon=0$, is about 4400. The theoretical critical Rayleigh number is, however, given as 1708 from the linear stability analysis of the hydrodynamic equations based on the Boussinesq approximation [24]. In our simulation, the collision process of the DSMC method is calculated in the sampling cell, which is about five times larger than the mean free path. It is reported, when the collision process is calculated in a region smaller than the mean free path, that the transition between conduction and convection is observed at around the hydrodynamic critical Rayleigh number of 1708 [17]. The onset of convection is thus found to be much influenced by the cell size. The distribution of the vertical velocity for $\varepsilon=0.029$ at $(y/L_y)=0.5$ and $(z/L_z)=0.5$ is shown in Fig. 2. The analytical velocity distribution obtained by the perturbation theory [24] is also shown. It is found that the good agreement between the DSMC results and the hydrodynamic theory is obtained again and the convection state is simulated qualitatively well.

IV. FLOW PATTERN TRANSITION

Typical patterns of temperature distribution at the midelevation, $(z/L_z)=0.5$, are shown in Figs. 3(a)–3(f). The tem-

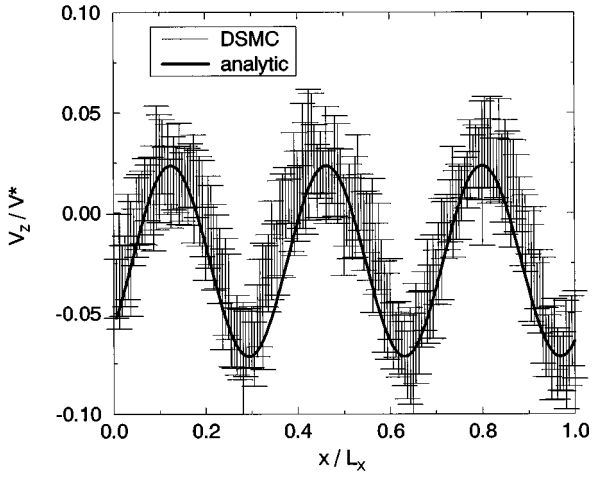

FIG. 2. Vertical velocity distribution in the steady state for $\varepsilon = 0.029$. DSMC results are obtained at $(y/L_y) = 0.5$ and $(z/L_z) = 0.5$ (midelevation) of the simulation region.

peratures are normalized so that the temperatures of the top and bottom walls are 0.0 and 1.0, respectively, and the isothermal contours for the nondimensional temperatures of 0.48, 0.54, 0.60, and 0.66 are shown in the horizontal plane. Figures 3(a)–3(d) are obtained during the process of increasing ε, while 3(e) and 3(f) are for decreasing ε. The heat conduction state for $\varepsilon = -0.224$ is shown in Fig. 3(a). The temperature distribution at the midelevation is almost homogeneous in the heat conduction state and it is indicated that no large-scale flow appears in the system. The convection state for $\varepsilon = 0.029$ is shown in Fig. 3(b). The temperature distribution at the midelevation corresponds clearly to the hexagonal flow pattern. Figures 3(a) and 3(b) are obtained at the steady state, and the stable hexagonal convection pattern is observed up to $\varepsilon = 0.680$ for increasing ε. One of the transient patterns for $\varepsilon = 0.842$ is shown in Fig. 3(c). In this case, the hexagonal convection pattern appears initially and evolves into a roll pattern. The stable roll pattern is observed in the steady state as shown in Fig. 3(d). It is found that the direction of the roll corresponds to one of the directions of the hexagonal pattern shown in Fig. 3(b). The transient pattern and the steady state for $\varepsilon = 0.214$ are shown in Figs. 3(e) and 3(f), respectively, for decreasing ε. The roll pattern is seen to be broken in Fig. 3(e), and the hexagonal pattern appears again in Fig. 3(f). For decreasing ε, the stable roll pattern is observed even at $\varepsilon = 0.463$. Although one of the directions of the hexagonal pattern corresponds to the direction of the roll shown in Fig. 3(d), the location of the hexagonal pattern is slightly different from that shown in Fig. 3(b).

The hexagonal and roll flow patterns shown in Figs. 3(b) and 3(d) are also observed in the experiments under non-Boussinesq conditions [22,25]. In our simulation, the temperature difference between the top and bottom walls is about 114 K for the theoretical critical Rayleigh number, and the temperature dependence of gas properties is not negligible. The stability of cellular convection flow and the temperature dependence of fluid properties have been discussed by Busse [26]. The Rayleigh numbers corresponding to the transition from hexagons to rolls and from rolls to hexagons are calculated to be about 5070 and 2840, respectively, by

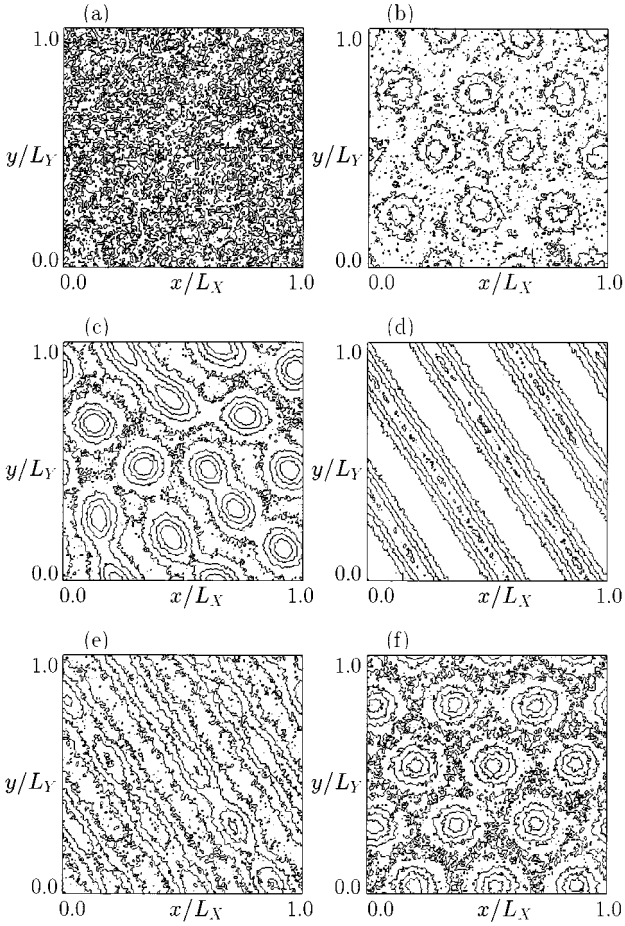

FIG. 3. Typical temperature distribution at the midelevation, $(z/L_z) = 0.5$, of the simulation region. Isothermal contours for the nondimensional temperature of 0.48, 0.54, 0.60, and 0.66 are shown in the horizontal plane: (a) steady state for $\varepsilon = -0.224$, (b) steady state for $\varepsilon = 0.029$, (c) transient state for $\varepsilon = 0.842$, (d) steady state for $\varepsilon = 0.842$, (e) transient state for $\varepsilon = 0.214$, and (f) steady state for $\varepsilon = 0.214$. (a)–(d) are obtained during the process of increasing ε, while (e) and (f) are obtained for decreasing ε.

Busse's method for our simulation conditions. These Rayleigh numbers observed in our simulations are about 7700 and 5700 from Fig. 1. It is thus found that not only the onset of convection but also the transition of convection patterns are influenced by the simulation cell size.

V. EFFECT OF CELL SIZE

The effect of cell size on the transition between heat conduction and convection is estimated by performing simulations with smaller sampling cells. The simulation region is a rectangular box with an aspect ratio of 2:2:1 in this case: 11.2 mm in horizontal directions and 5.6 mm in vertical direction. The number of sampling cells is $200 \times 200 \times 100$. A side length of the sampling cell is thus smaller than the mean free path, while a diagonal length of the cube is almost the same as the mean free path. Initial and boundary conditions are the same as the previous simulations with the large aspect ratio. The bottom wall temperature ranges from 150 K–300 K. The number of simulation particles is 1.6×10^8 and the simulations are performed on Intel Paragon with

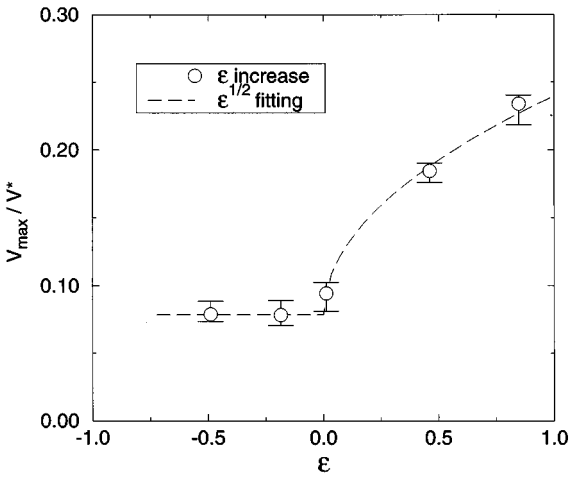

FIG. 4. Maximum vertical velocity in the steady state as a function of ε. The DSMC data are obtained by the simulations with smaller sampling cells. The data points show a long-time average in the steady state and the error bars indicate the range of data distribution. The dashed line indicates a fitting curve of $\varepsilon^{1/2}$.

256 processors in this case. The time step is 0.4 of the mean free time and a sampling is performed in every three simulation time steps, and a flow field is obtained by an average of 50 samplings. The time step size and the number of samplings are slightly smaller than those in the preceding case.

The maximum flow velocity in the vertical direction, which corresponds to Fig. 1 for the case with larger sampling cell, is shown in Fig. 4. The transition between heat conduction and convection around $\varepsilon=0$ and the growth rate of the flow velocity at $\varepsilon>0$ are simulated well. The critical Rayleigh number, which is obtained as about 1800 in this case, is in good agreement with the theoretical value. The calculated Rayleigh number also agrees well with that obtained by the two-dimensional DSMC simulation [17]. Although the transition of convection patterns is not seen in Fig. 4, it is confirmed that the onset of convection is influenced by the sampling cell size.

VI. SUMMARY

In this paper, the three-dimensional RB conduction-convection system has been simulated using the DSMC method. Although several convection patterns are already known in the experiments and model calculations [1–3], we use the particle simulation method to observe the hexagonal and roll patterns and the hysteresis in their transition.

The DSMC method is developed for solving the Boltzmann equation, and is appropriate for simulating a flow field where the Navier-Stokes equations of continuum gas dynamics are not valid. Since the DSMC method is a statistical method, a large number of particles are necessary to obtain transient flow fields especially for three-dimensional simulations. Recent development of computers, however, enables us to simulate various kinds of flow problems using the DSMC method [19]. This technique is numerically stable and easily applied to complicated flow geometries. The fluctuations of field variables due to the molecular motion, which are associated with macroscopic flow phenomena [18], are obtained as well as average flow fields. Our results demonstrate that macroscopic flow transitions and instabilities are simulated from the molecular level. It is indicated that the microscopic origin of macroscopic flow phenomena can be studied using particle simulation methods.

ACKNOWLEDGMENT

The authors gratefully acknowledge Mr. Hideki Noguchi of CRC Research Institute, Inc. for parallelization of the DSMC program.

[1] G. Ahlers, Physica D **51**, 421 (1991).
[2] M. C. Cross and P. C. Hohenberg, Rev. Mod. Phys. **65**, 851 (1993).
[3] W. Pesch, CHAOS **6**, 348 (1996).
[4] M. Mareschal and E. Kestemont, J. Stat. Phys. **48**, 1187 (1987).
[5] M. Mareschal and E. Kestemont, Nature (London) **239**, 427 (1987).
[6] D. C. Rapaport, Phys. Rev. Lett. **60**, 2480 (1988).
[7] M. Mareschal, M. M. Mansour, A. Puhl, and E. Kestemont, Phys. Rev. Lett. **61**, 2550 (1988).
[8] A. Puhl, M. M. Mansour, and M. Mareschal, Phys. Rev. A **40**, 1999 (1989).
[9] J. A. Given and E. Clementi, J. Chem. Phys. **90**, 7376 (1989).
[10] T. Watanabe and H. Kaburaki, Phys. Rev. E **54**, 1504 (1996).
[11] H. A. Posch, W. G. Hoover, and O. Kum, Phys. Rev. E **52**, 1711 (1995).
[12] O. Kum, W. G. Hoover, and H. A. Posch, Phys. Rev. E **52**, 4899 (1995).
[13] W. G. Hoover and O. Kum, Mol. Phys. **86**, 685 (1995).
[14] A. L. Garcia, in *Microscopic Simulations of Complex Flows*, edited by M. Mareschal (Plenum, New York, 1990), p. 177.
[15] S. Stefanov and C. Cercignani, Eur. J. Mech. B **11**, 543 (1992).
[16] A. Garcia and C. Penland, J. Stat. Phys. **64**, 1121 (1991).
[17] T. Watanabe, H. Kaburaki, and M. Yokokawa, Phys. Rev. E **49**, 4060 (1994); **51**, 3786 (1995).
[18] T. Watanabe, H. Kaburaki, M. Machida, and M. Yokokawa, Phys. Rev. E **52**, 1601 (1995).
[19] G. A. Bird, *Molecular Gas Dynamics and the Direct Simulation of Gas Flows* (Clarendon, Oxford, 1994).
[20] S. Chapman and T. G. Cowling, *The Mathematical Theory of Non-Uniform Gases* (Cambridge University Press, Cambridge, England, 1970).
[21] M. Dubois, P. Berge, and J. Wesfried, J. Phys. (France) **39**, 1253 (1978).
[22] S. Ciliberto, E. Pampaloni, and C. Pérez-García, Phys. Rev. Lett. **61**, 1198 (1988).
[23] J. K. Bhattacharjee, *Convection and Chaos in Fluids* (World Scientific, Singapore, 1987).
[24] S. Chandrasekhar, *Hydrodynamic and Hydromagnetic Stability* (Clarendon, Oxford, 1961).
[25] P. L. Silveston, Forsch. Ing. Wes. **24**, 29 (1958).
[26] F. H. Busse, J. Fluid Mech. **30**, 625 (1967).